IEEE Access
Multidisciplinary | Rapid Review | Open Access Journal

Received April 2, 2021, accepted May 2, 2021, date of publication May 7, 2021, date of current version May 21, 2021.

Digital Object Identifier 10.1109/ACCESS.2021.3078415

Non-Destructive Water Leak Detection Using Multitemporal Infrared Thermography

MOHAMED YAHIA[1,2], RAHUL GAWAI[1], TARIG ALI[1,3], (Senior Member, IEEE), MD. MARUF MORTULA[3], LUTFI ALBASHA[4], (Senior Member, IEEE), AND TAHA LANDOLSI[5]

[1]GIS and Mapping Laboratory, American University of Sharjah, Sharjah, United Arab Emirates
[2]Laboratoire de recherche Modélisation analyse et commande de systèmes (MACS), Ecole Nationale d'Ingénieurs de Gabes (ENIG), Université de Gabes, Avenue Omar Ibn Elkhattab 6023, Tunisia
[3]Department of Civil Engineering, American University of Sharjah, Sharjah, United Arab Emirates
[4]Department of Electrical Engineering, American University of Sharjah, Sharjah, United Arab Emirates
[5]Department of Computer Science and Engineering, American University of Sharjah, Sharjah, United Arab Emirates

Corresponding author: Mohamed Yahia (myahya@aus.edu)

This work was supported by the Smart City Research Institute, American University of Sharjah, United Arab Emirates, under Grant EN0-282 and Grant EN0-284.

ABSTRACT Waterleakage detection and localization in distribution networks pipelines is a challenge for utility companies. For this purpose, thermal Infrared Radiation (IR) techniques have been widely applied in the literature. However, the classical analysis of IR images has not been robust in detecting and locating leakage, due to presence of thermal anomalies such as shadows. In this study, to improve the detection and location accuracy, a digital image processing tool based on multitemporal IR is proposed. In multitemporal IR analysis, the variation of soil's temperature due to field temperature can be obtained; and hence; estimating variations due to water leakage would be more accurate. An experimental setup was built to evaluate the proposed multitemporal IR water leak detection method. In order to consider the temporal temperature variation due to water leakage and mitigate the field temperature effects, a luminance transformation of the IRimages was introduced. To determine the temporal temperature variation of the soil's surface due to the leakage, several metrics have been considered such as the difference, the ratio, the log-ratio and the coefficient variation (CV) images. Based on the experimental results, the log-ratio and the CVimages were the most robust metrics. Then, based on log-ratio or the CV image, a temporal variation image (TVI) that traduces the temporal IR luminance variation was introduced. The analysis of the TVI image showed that the CV image is less noisy than the log-ratio image, and can more accurately locate the leakage. Finally, based on TVI histogram, a threshold was defined to classify the TVI image into leakage/non-leakage areas. Results showed that the proposed method is capable of accurately detecting and locating water leakage, which is an improvement to the false detections of spatial thermal IR analysis.

INDEX TERMS Sustainable development goals (SDG), non-destructive evaluation (NDE), infrared thermography, water leak detection, multitemporal analysis.

I. INTRODUCTION

Clean drinking water and environmental degradation fighting are two challenges addressed by the Sustainable Development Goals (SDG) [1]. Water leakage in the distribution network is one of potential causes preventing the achievement of these goals. In fact, water leaks cause significant losses of drinking water and significant deterioration of the water quality within the supply system while large leaks can potentially cause flooding and disrupts the quality of the urban environment.

The associate editor coordinating the review of this manuscript and approving it for publication was Wuliang Yin.

Various nondestructive evaluation (NDE) leak detection techniques have been proposed in the literature [2]–[19]. Table 1, presents a comparison of the performance of some basic leak detection techniques. In [2], the leak detection technologies are categorized into external/internal to the pipelines-based methods. In [3], the authors grouped them into non-numerical, numerical and time domain, frequency domain analysis. The Closed-Circuit Television (CCTV) is a well-known technique for the leak detection [2]. The system includes a remote-controlled platform and a camera mounted on a robot moving between two manholes inside the pipeline [2]. In acoustic technology, the acoustic sensors such as pressure sensors, accelerometers, or hydrophones, are

TABLE 1. Performance of some leak detection techniques.

Method	Advantage	Disadvantage
Closed-circuit television (CCTV)	Applied to sewer and storm water pipes Used for water main rehabilitation	Time-consuming, labor intensive and low reliability in detecting leaks Accuracy is dependent on the user's experience [2].
Acoustic Emission	Real time [16], high detection and localization accuracy [2]	Signals are influenced by the type of pipe materials and pipeline section [16] Sensitive to background noise [4]. Requires a great number of long pipelines [2] Insensitive to large leaks [17].
Ground penetration radar	Applied to various pipe materials such as concrete, stone, plastic, masonry materials, wood and some ceramics. Not limited by pipe size [18]	influenced by the type of soil Ineffective for inhomogeneous soil. influenced by the moisture of soil [7] It is difficult to interpret the results [12].
Fiber optics	Provides accurate leakage detection and location [19]. Immunity to electrical noise, long-term measurement stability, corrosion resistant properties and provides long-distance sensing capabilities with many measurement points through hone optical fiber line [15]	High cost can only be deployed for monitoring linear pipelines [15, 2]
Infrared thermography	Large areas to be investigated Near-real time Low cost It can be used in day or night time. Independent of pipe material type and size [7].	Certain level of expertise is also required to analyze the image. Influenced by the moisture of soil [7] affected by weather conditions [16]

distributed on the pipeline or inside it [4]. They sense leakage's mechanical noise. In ground penetration radar (GPR), radiofrequency RF waves are transmitted from the antenna. The backscattered signal is recorded to create a 3D profile of underground layers. The leakage is identified by the irregularities in the 3D profile due to the underground voids created by the leaks [5]. In fiber optics techniques, since leakages from pipeline cause local temperature anomalies, optical fiber line installed over the entire pipeline can detect the leakage by taking temperature measurements [6].

Infrared Radiation (IR) thermography remote sensing which relies on variations in thermal emission provides powerful means for large-scale detection of leaks [5], [7]–[14]. Water present in soil generates latent heat losses through evaporation. Based on this concept, a large number of remote sensing experiments involving IR sensors have been conducted for detecting water leaks [5], [7]–[14]. In addition, IR enables relatively large areas to be investigated effectively in near-real time. It is also independent of pipe material type and size [5]. These advantages make use of the IR camera overcomes limitations associated with currently leak detection methods. The reliability of IR in detecting leaks in buried water pipes is studied in [8]. Nevertheless, IR water leak detection techniques are based on the identification of thermal anomalies of a scalar IR image acquired in a fixed time. However, despite the advantages of scalar IR, the detection accuracy was quite low due to false positives generated by other thermal anomalies such as shadows [5], [12]–[14].

In this study, the false detection problem of classical scalar IR technique has been addressed. The novelty is the exploitation of the temporal temperature variation caused by the leakage rather than combining the IR with other technologies. In fact, in addition to 2D spatial thermal anomalies, water leaks can also generate temporal variation of the thermal profile of the leakage surface. Hence, temperature variation in temporal IR is an important parameter that characterizes ground change [20]–[22]. Recently, the temporal IR is exploited to detect buried mines [21]. Due to the different thermal properties between soil and mine, the temperature of soil surface above mine differs from its surroundings during a heating-cooling procedure. The IR sequences are analyzed visually after the cooling process. In the 2D thermograms, a 'hot spot' appeared on the surface above mine. In addition, the authors demonstrated that, after the cooling process, the slowest temperature decrease of the soil is above the mines. Nevertheless, only 2D thermal anomalies are exploited to identify the positions of mines whereas the temporal information is ignored. On the other hand, in the proposed study, a deep study of the temporal variation of the temperature profile of leakage surface, a multitemporal high resolution IR water leak detection technique is proposed. After that, based on the properties of the temporal thermal profiles of leakage zones, a water leakage technique has been proposed. Using this method, the variation of the soil's temperature due to field temperature can be obtained; and hence; estimating the variations due to water leakage would be more accurate.

This paper is organized as follows: In section II, the experimental data are introduced. Section III presents the problem formulation. In section IV, the proposed leak detection method is detailed. The results and discussions are given in

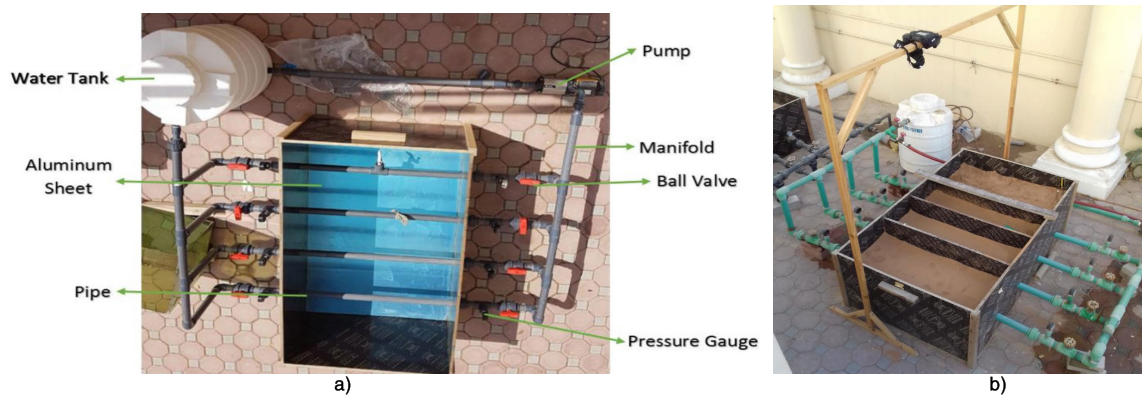

FIGURE 1. Experiment setup: Top view.

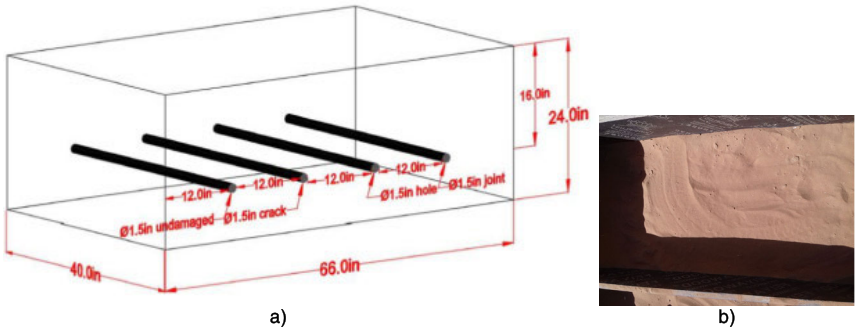

FIGURE 2. Experiment setup: a) Dimensions, b) Initial image.

sections V and VI, respectively. Finally, Section VII presents the conclusions of this study.

II. EXPERIMENTAL DATA

The experimental setup, shown in Figs. 1 and 2 simulates a section of water distribution network (WDN) in United Arab Emirates(UAE). A dune sand filled box with plastic pipes built to investigate the effectiveness of the proposed multitemporal IR for leak detection. The boxes were filled three years before realizing the experiments (March 2018). A compaction process has been realized as described in [7]. The boxes are situated in open air to resemble as much as possible the real conditions of UAE environment (i. rain, worms and other animals). Tables 2 shows the parameters of the WDN pipes, camera, and images. For test1 and test2 datasets, the leakage carried out at 11h am and 2pm respectively while the soil was exposed to the sun (except the shadowed area as seen in Fig. 2b).

IR detection was possible after 40 min of water leakage (i.e. 11.40 am for test1 and 2.40 pm for test2). This duration is comparable to that reported in [11]. For test1 datasets, at 11hminam: i) all the experiential setup is shadowed by the neighboring buildings; therefore, the overall temperature of the soil was expected to decrease with time (see Fig. 1b). ii) The initial temperature of the shadowed area in Fig. 2b) was lower than that in other parts of the soil (i. e. temperature anomaly).

A. DATA SET

Figs. 3 and 4display the thermograms of test1 and test2 datasets, respectively. For image processing purpose, thermograms are captured in grayscale RGB (red, green and blue) format where R, G and B layers are equal. Hence, only one layer is selected for image processing. The grayscale format ensures a bijection between the temperature and the luminance. On the other hand, false colour palettes do not ensure a bijection between the values of RGB layers and the temperature. The processing of one layer of false colour images (e. g. G layer in [5]) is not optimal. False colour images can be displayed for perception purposes to increase the contrast of the thermograms as illustrated in Fig. 5.

III. PROBLEM FORMULATION: SPATIAL-BASED IR LEAK DETECTION

In classical IR techniques, a single thermogram captured at a fixed time is analyzed visually or processed to detect the leakage area. The false color palettes can be used to enhance the contrast of the thermograms.

Fig. 5 visually shows the acquired thermograms using false colors. Fig. 6b) displays the temperature profiles of leakage and non-leakage areas. The leakage is characterized by a lower temperature than the soil one.

In addition to the water leakage, a significant temperature drop due the shadow is perceived as seen in Figs. 6a). When

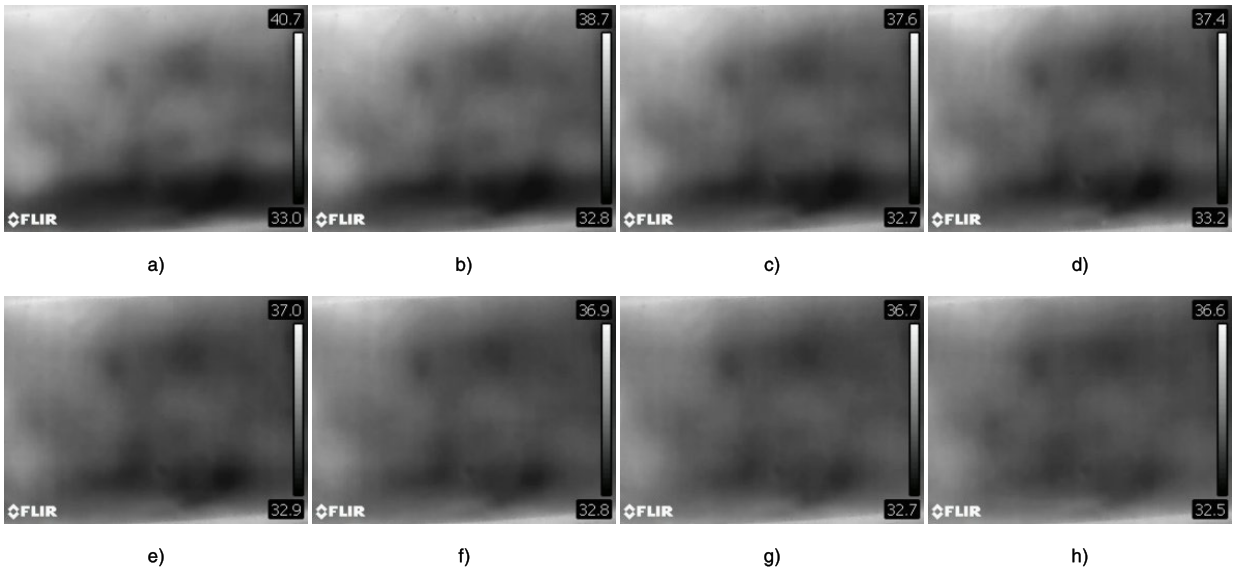

FIGURE 3. Multitemporal raw IR images ti = 40min+T∗i (T = 10min, n = 1: 8) a) t1, b) t2, c) t3, d) t4, e) t5, f) t6, g) t7, h) t8. The temperature ranges have been set automatically by the camera.

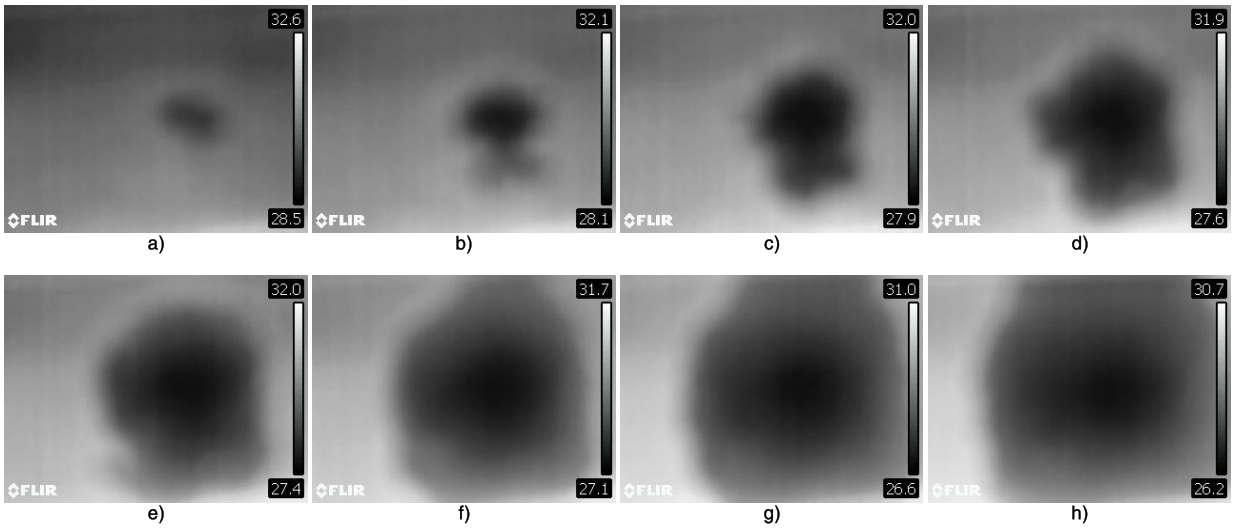

FIGURE 4. Multitemporal raw IR images ti = 40min+T∗i (T = 1min, n = 1: 8) a) t1, b) t2, c) t3, d) t4, e) t5, f) t6, g) t7, h) t8. The temperature ranges have been set automatically by the camera.

the thermogram is spatially low contrasted or displays small temporal changes, the visual inspection can fail to identify leakage areas. To resolve this problem, image processing techniques that are based on objective criteria (i. e. quantitative metrics) are applied [5], [9], [10], [22]–[26]. Histogram based algorithms are commonly applied, such as histogram equalization [23] and [25].

Fig. 6c) displays the histograms of the leakage, non-leakage and the shadowed areas that are calculated from the rectangular zones(see Fig.6a) where 'TH' is the threshold used to segment the IR image into leakage and non-leakage areas. It can be observed that leakage and non-leakage areas can be discerned. Nevertheless, leakage and shadowed areas have overlapped luminance values. As a result, the spatial luminance-based techniques are not able to discern them [5], [9], [10], [23]–[25].

For TH = 80, leakage areas can be identified in the segmented image as seen in Fig 6d). Nevertheless, wide false positive area corresponding to the shadowed zone is also detected. In this study, to reduce the misinterpretations and increase the competitiveness of IR technology, the multitemporal IR is employed instead of using other technologies such as multispectral [12], visible sensors [11], [12], GPR [5].

IV. TEMPORAL-BASED IR LEAK DETECTION

For optimal exploitation of the advantages of IR, the repeat pass IR is applied. The originality of the method is the detection of leaks by exploiting the time variation of temperature. Since the leak location has lower temperature than the surrounding soil, this will cause its temperature decrease continuously. Hence, the highest temperature variation surface

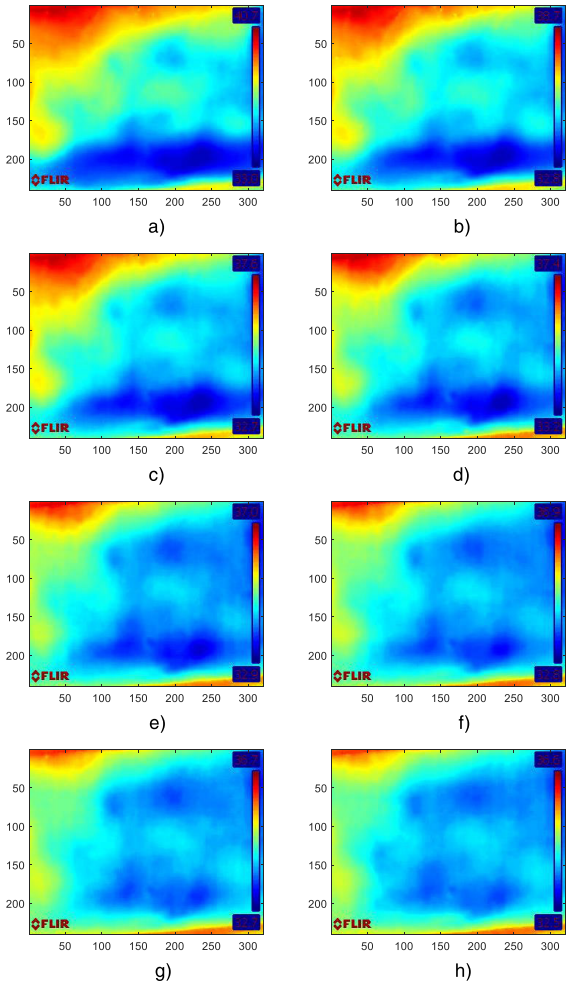

FIGURE 5. Multitemporal false colour IR images, a) t1, b) t2, c) t3, d) t4, e) t5, f) t6, g) t7, h) t8.

is above the leakage. The objective is to define a metric that emphasize such temporal temperature variation.

A. LUMINANCE TRANSFORMATION

Fig. 6b) displays the temporal luminance profiles of the leakage and the non-leakage areas. Due to water leakage, the width W of the leakage area has increased(W2 > W1 in Fig 6b). Nevertheless, the decrease of the soil's temperature is not due to leakage only but it is also due to the field temperature, as explained in section II. To emphasize the temporal temperature variation, the difference between the successive IRimages is displayed in Fig. 7. It can be observed that important changes are essentially due to field temperature rather than leakage since the leakage area is not highlighted. Hence, to emphasize the leakage temperature variation and mitigate the effects of the field temperature (i. e. the absolute value of the luminance), the dynamic ranges of the luminance of all multitemporal IR images are shifted. Let $\mathcal{L}(t_i)$ be the luminance of the thermograms and $\mathcal{L}_s(t_i)$ be the shift-transformed luminance at time t_i $(i = 1, \ldots, 8)$

$$\mathcal{L}_s(t_i) = \mathcal{L}(t_i) - \min\left\{\mathcal{L}(t_i)\right\} \quad (1)$$

TABLE 2. Experimental Setup Parameters.

Pipe parameters	Value	Value
Material	Polypropylene (PPR)	Polypropylene (PPR)
Diameter	1.5 in	1.5 in
Depth	16 in	16 in
Leak	Faulty joint	Faulty joint
Water parameters	**Value**	**Value**
Temperature	23°C	21°C
Pressure	0.3Pa	0.5Pa
Water leakage	11am	14am
Soil	**Value**	**Value**
Type	Dune sand	Dune sand
Compaction	90%	90%
Time of sand lying	March 2018	March 2018
Density	(1689.41 kg/m3)	(1689.41 kg/m3)
IR camera parameters	**Value**	**Value**
Type	FLIR T420	FLIR T420
Wavelength	7.5-13.0µm	7.5-13.0µm
Emissivity	0.98 (dry soil)	0.98 (dry soil)
Height from the soil	1.5 m	1.5 m
IR image parameters	**Value**	**Value**
Start	11.40am	2.40pm
Temporal resolution	1 image/10 min	1 image/ min
Spatial resolution	0.15×0.15cm^2	0.15×0.15cm^2

Fig. 8 displays $\mathcal{L}(t_i)$ images in which the effect of the initial absolute value of the luminance has been mitigated (i.e. in comparison with Fig. 5). As a result, the luminance variation in Fig. 8 is essentially due to the leakage. The objective is to exploit such variation for water leakage detection and localization.

Fig. 9 displays the mean $\mathcal{L}_s(t_i)$ of leakage, non-leakage and shadowed areas as a function of the time (t_i). Due to water leakage, the transformed luminance $\mathcal{L}_s(t_i)$ decreases with time. This decrease is more rapid in the leakage area since it is closer to the leakage location. These observations, have been considered in the development of the water leakage detection method.

B. QUANTITATIVE METRICS

The objective here was to quantify the time variation of the transformed luminance $\mathcal{L}_s(t_i)$. Various metrics have been evaluated.

a: THE DIFFERENCE IMAGE

As stated previously, this metric fails to identify the leakage as seen in Fig. 7.

b: THE RATIO IMAGE

Unlike the difference, the ratio image was sensitive to the absolute value of the luminance. In this study, the transformed luminance $\mathcal{L}_s(t_i)$ is used. The leakage water could have lower or higher (by heating water [26]) temperature than that of

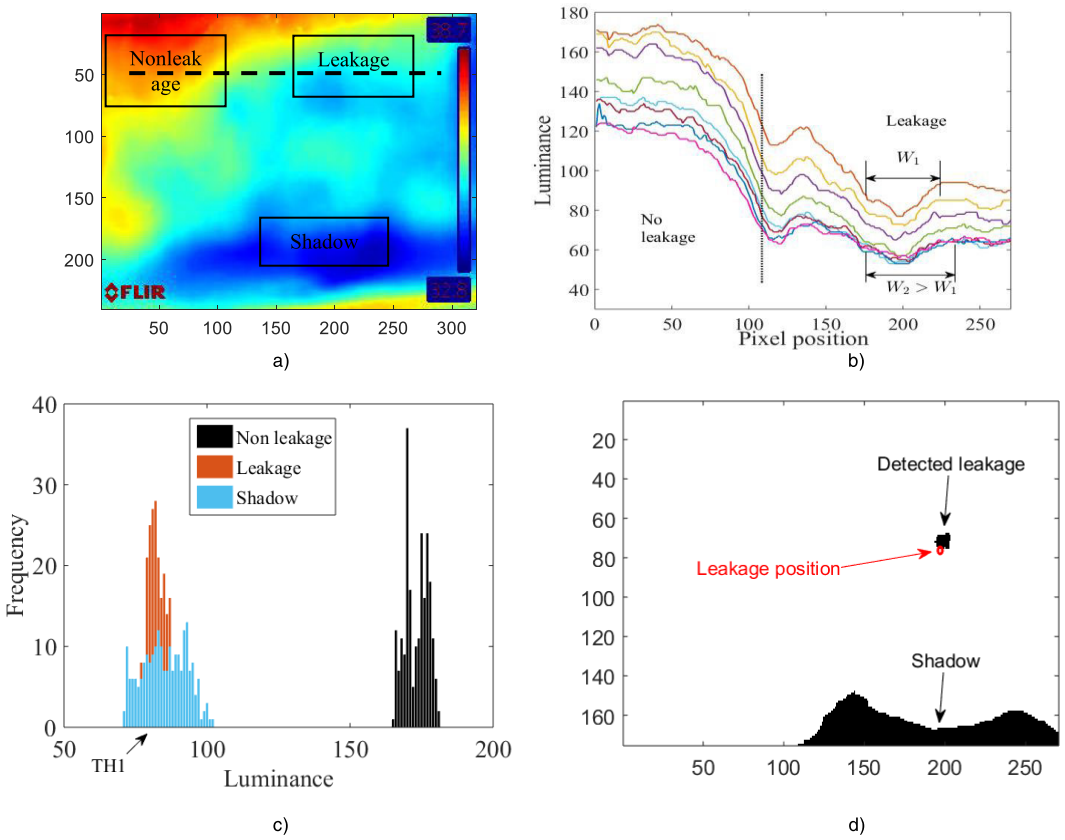

FIGURE 6. a) TIR image of Fig. 4b), b) Multitemporal luminance profiles of dashed line a), c) Histograms of the rectangular zones in a), d) Classified image TH = 80.

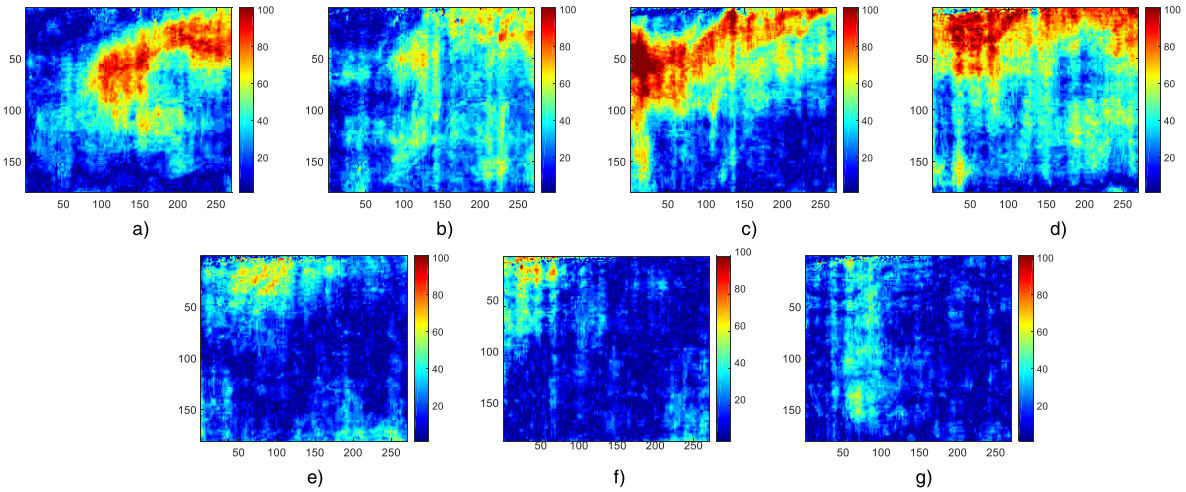

FIGURE 7. Difference IR images between successive acquisitions.

soil. To highlight the temperature changes in both cases, the following ratio image was defined:

$$\Re\left(t_i\right) = \frac{\mathcal{L}_s\left(t_{i+1}\right)}{\mathcal{L}_s\left(t_i\right)} + \frac{\mathcal{L}_s\left(t_i\right)}{\mathcal{L}_s\left(t_{i+1}\right)} \tag{2}$$

Figs. 10 displays the ratio images between successive transformed IR images. It can be observed that the ratio image has identified the leakage areas from the non-leakage and the shadowed areas. In fact, as shown in Fig. 9, the leakage area is characterized by a more rapid decrease of $\mathcal{L}_s\left(t_i\right)$ than the shadowed area. On the other hand, both leakage and non-leakage areas are characterized by a decrease of $\mathcal{L}_s\left(t_i\right)$. Nevertheless, as shown in Fig. 9, the leakage area has significantly lower $\mathcal{L}_s\left(t_i\right)$ values. Based on these results, the ratio

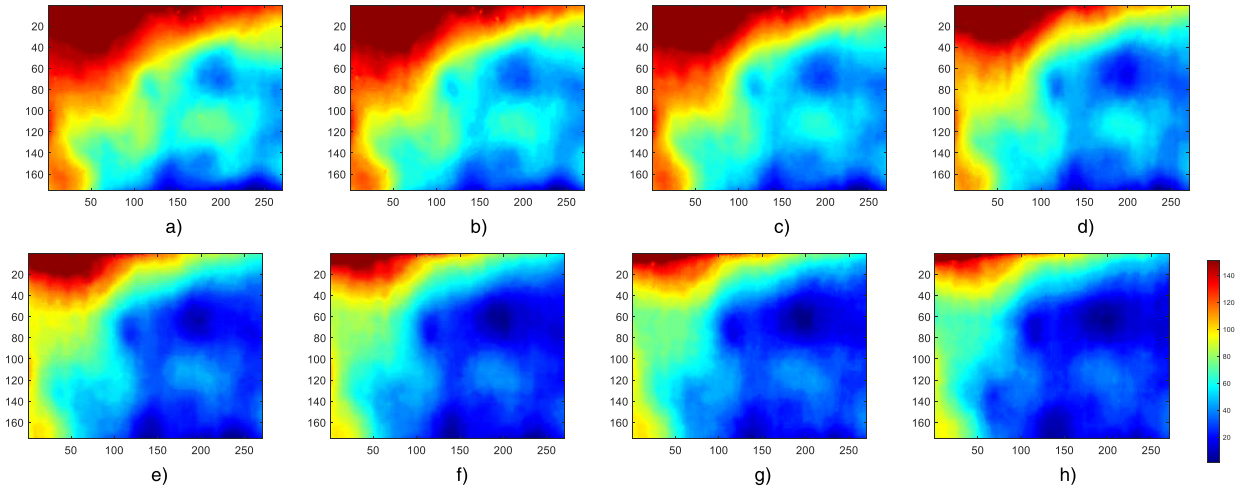

FIGURE 8. Multitemporal transformed IR images $\mathcal{L}_s(t_i)$.

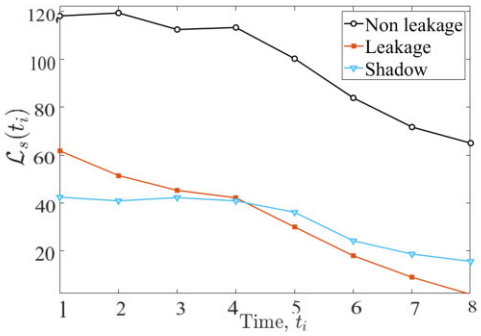

FIGURE 9. Temporal evolution of mean($\mathcal{L}_s(t_i)$) of leakage, non-leakage and shadowed areas.

image is capable of discerning leakage from non-leakage and shadowed areas. Nevertheless, the contrast of the ratio image is low as shown in Fig. 10.

c: THE LOG-RATIO IMAGE:

The log-ratio image is defined as

$$\mathcal{R}_l(t_i) = \left|\log \frac{\mathcal{L}_s(t_{i+1})}{\mathcal{L}_s(t_i)}\right| = \left|\log \frac{\mathcal{L}_s(t_i)}{\mathcal{L}_s(t_{i+1})}\right| \quad (3)$$

Figs. 11 displays the log-ratio images. It can be observed that this metric has improved the visual detection compared to the ratio image. Fig. 12 demonstrates that the application of the log-ratio without the transformation (1) would fail to identify the leakage area. To assess the temporal variation of the transformed IR images, the mean of the log-ratio images was used

$$\bar{\mathcal{R}}_\ell = \frac{1}{N-1}\sum_{i=1}^{N-1}\mathcal{R}_l(t_i) \quad (4)$$

where N is the number of IR images. Fig. 13a) displays $\bar{\mathcal{R}}_\ell$ image. Fig. 13b) displays $\bar{\mathcal{R}}_\ell$ histograms of the leakage, non-leakage and the shadowed areas. Unlike the spatial analysis in Fig. 6c), it can be observed that $\bar{\mathcal{R}}_\ell$ image discerned the leakage area.

d: THE COEFFICIENT VARIATION

The Coefficient Variation (CV) is commonly applied in synthetic aperture radar images as a measure of the spatial variability of the image [27]. In this study, the temporal variability is assessed instead. The CV of the pixel (x, y) is defined as

$$CV(x,y) = \frac{std\left(\mathcal{L}_s(x,y,1:N)\right)}{mean\left(\mathcal{L}_s(x,y,1:N)\right)} \quad (5)$$

where *std* is the standard deviation.

Fig. 14a) displays CV image. Since the leakage area is characterized by a higher temporal variability than the shadow and the non-leakage areas (as shown in Fig. 9), CV image has successfully emphasized the leakage. It can be observed also that the CV image is less noisy than the $\bar{\mathcal{R}}_\ell$ image. Unlike the spatial analysis in Fig. 6c), the histograms displayed in Fig. 14b) show that using an appropriate threshold can help to discern the leakage location.

V. PROPOSED LEAK DETECTION METHOD

The leakage detection and localization is formed as a binary classification problem. In the classified image, a binary "1" is assigned to leakage and binary "0" is assigned to non-leakage pixels. Consequently, the locations and the extent of leakage can be easily identified.

The proposed approach, which is described in Fig. 15 is composed of the following steps:

- Acquisition of multitemporal IR dataset.
- TVI image computation
- Histogram determination
- Derivation of the threshold.
- Generation of the classified image.

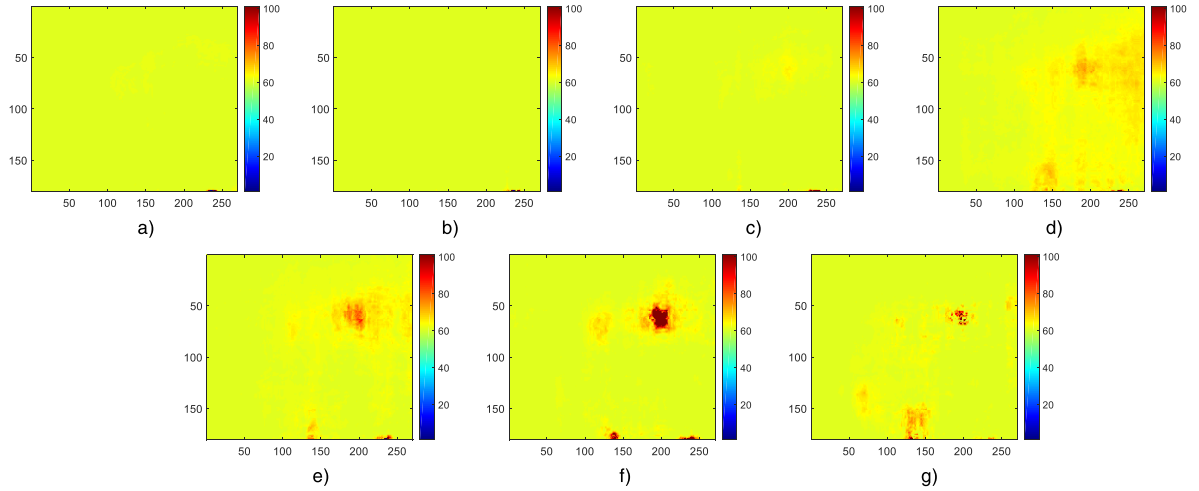

FIGURE 10. Ratio $\mathcal{R}(t_i)$ between the successive acquisitions (×30).

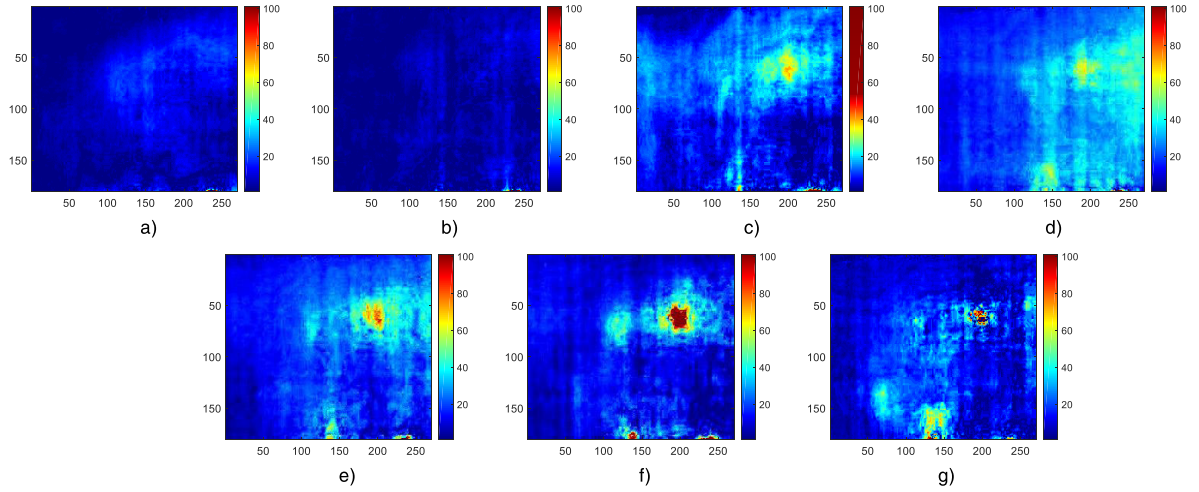

FIGURE 11. Log-ratio images $\mathcal{R}_\ell(t_i)$ (×100).

A. ACQUISITION OF MULTITEMPORAL IR DATASET

The first step of the proposed leakage detection technique is the acquisition of the multitemporal IR dataset as described in section II.

B. APPLY THE TRANSFORMATION $\mathcal{L}_s$

To mitigate the effect of time variation of field temperature, a luminance transformation ($\mathcal{L}_s$) is used.

C. COMPUTE TVI IMAGE

In order to determine the temporal variation of the soil temperature, due to leakage, the TVI image was computed. Two expressions have been proposed in this study for TVI image computation, TVI $= \bar{\mathcal{R}}_\ell$ (4) and TVI $=$ CV (5).

D. HISTOGRAM DETERMINATION

As demonstrated in TVI histograms in Figs. 13b) and 14b), the leakage area is characterized by high temporal temperature variation (i.e. high TVI values). Hence, TVI histogram is used to define the threshold and identify high TVI values.

E. DERIVATION OF THE THRESHOLD

To detect and locate the leakage zone, the proposed method was used successfully by applying thresholds. The threshold is derived by visually analyzing the TVI histogram. After that, the threshold is set to select high TVI values.

F. GENERATION OF THE CLASSIFIED IMAGE

Leakage and non-leakage pixels are identified by comparing each pixel of TVI image with the threshold. If the TVI pixel value is higher than the threshold "TH" it will be assigned to the non-leakage class.

$$Class\,(i,j) = \begin{cases} 1\ (Leakage) & if\ TVI\ (i,j) > TH \\ 0\ (Non-leakage) & elsewhere \end{cases} \quad (6)$$

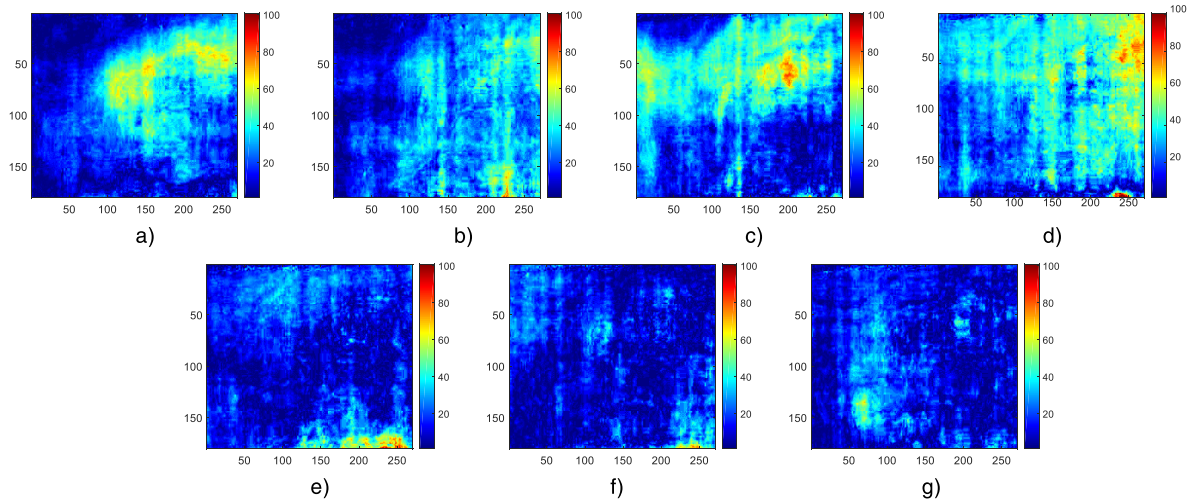

FIGURE 12. Log-ratio images without the application of the transformation $\mathcal{L}_s$ (×100).

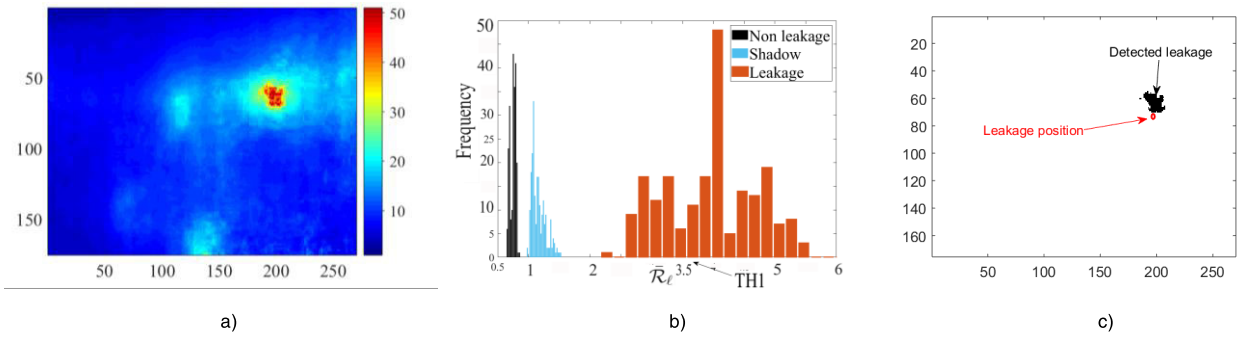

FIGURE 13. a) $\bar{\mathcal{R}}_\ell$ Image (×10), b)Histograms of $\bar{\mathcal{R}}_\ell$, c) classified image leakage/non-leakage areas TH1 = 3.5.

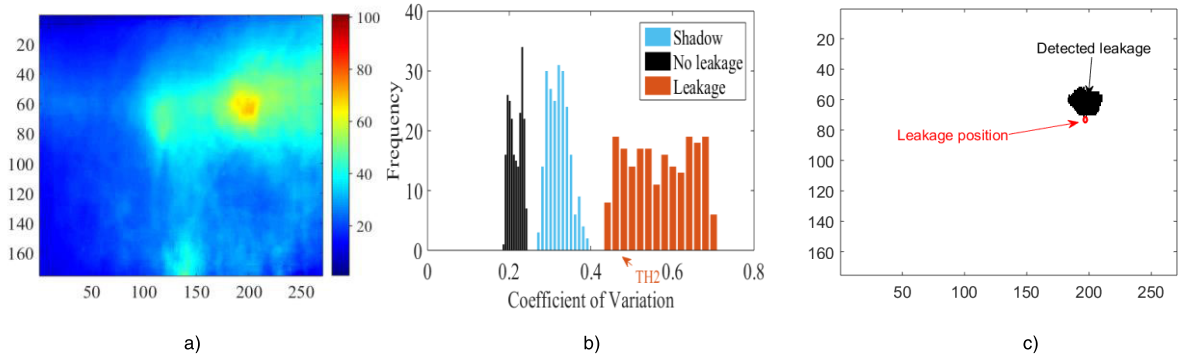

FIGURE 14. a) CV Image (×100), b) Histograms, c) classified image leakage/non-leakage areas TH2 = 0.6.

VI. RESULTS

In this section, the performance of the proposed multitemporal IR leakage detection technique is assessed using test 1 and test 2 datasets.

A. TEST 1 DATASET

For TVI = $\bar{\mathcal{R}}_\ell$ and fornon-leakage area, TVI ≈ 0.8. For shadow area, TVI ≈ 0.8 and for leakage area, TVI ≈ 4. The selected threshold is TH = 3.5. Fig. 12c) displays the classified leakage/non-leakage image. It can be observed that multitemporal IR analysis detected one potential leakage location without false positives.

For TVI = CV, fornon-leakage area, TVI ≈ 0.22, for shadow area TVI ≈ 0.35 and for leakage area TVI ≈ 0.65. The selected threshold is TH = 0.6. Fig. 14c) displays the classified image using CV metric. It is evident that the CV

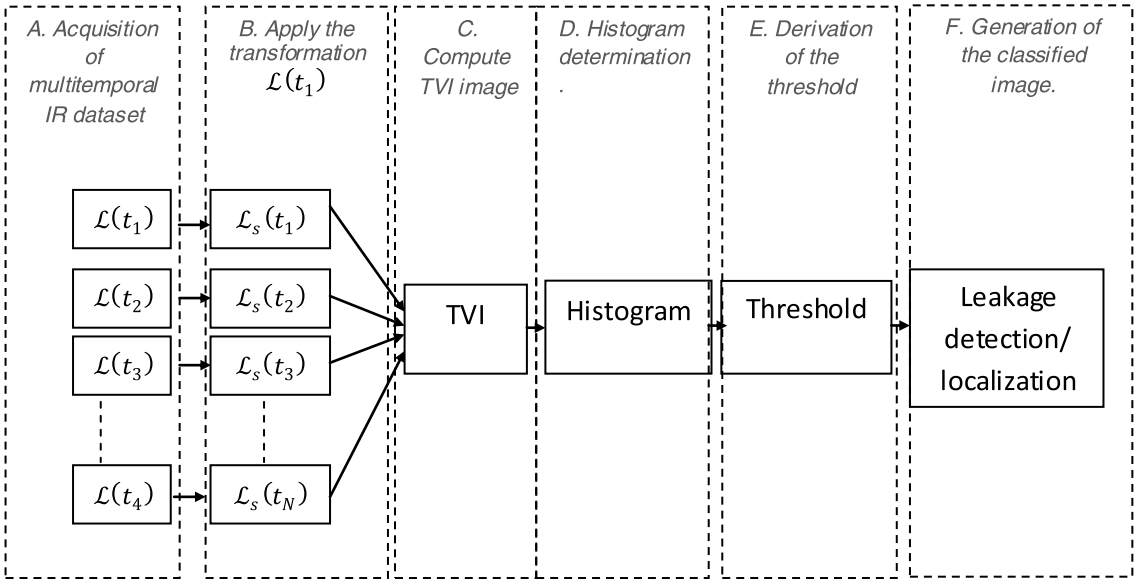

FIGURE 15. Flowchart of the proposed temporal IR image-based leakage and localization technique where the Temporal Variation Image TVI is TVI = $\bar{\mathcal{R}}_\ell$ or TVI = CV.

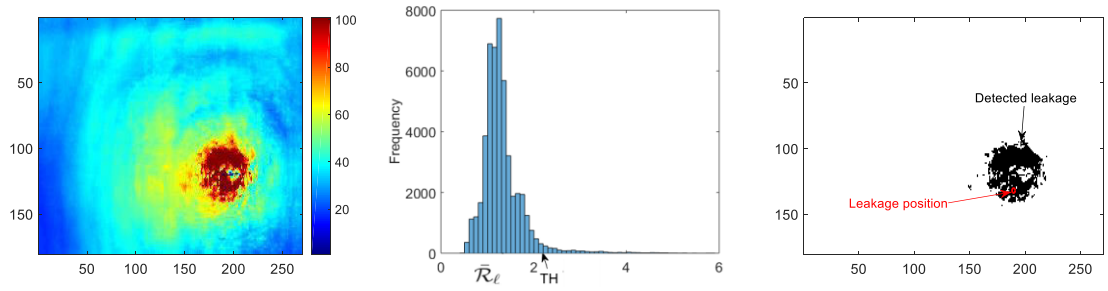

FIGURE 16. a) $\bar{\mathcal{R}}_\ell$ Image (×30), b) Histograms of $\bar{\mathcal{R}}_\ell$, c) classified image leakage/non-leakage areas TH1 = 2.5.

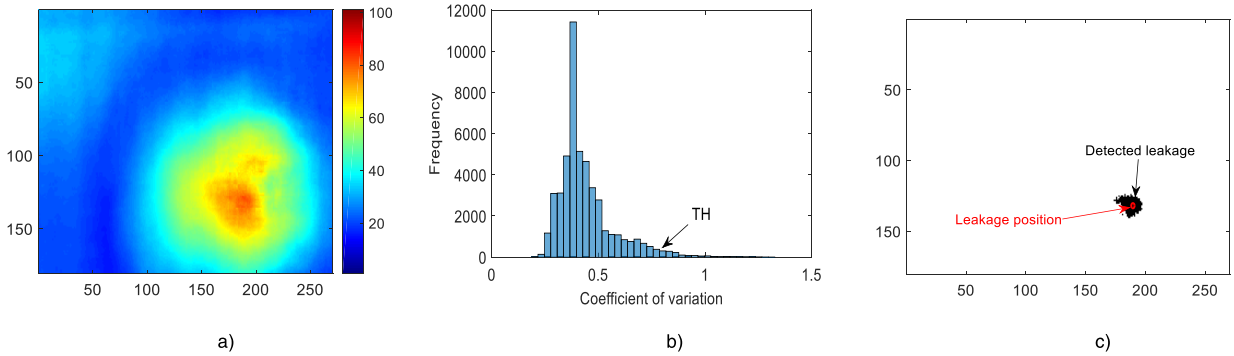

FIGURE 17. a) CV Image (×100), b) Histograms, c) classified image leakage/non-leakage areas TH2 = 0.75.

identified the leakage area, which is more compact than that detected by the log-ratio metric.

Field measurements of the distances between the leakage location and the center of the detected leakage zone was about 1 cm, in both cases.

B. TEST 2 DATASET

Figs. 16a) and 17a) display TVI = $\bar{\mathcal{R}}_\ell$ and TVI = CV images, respectively. It can be observed that leakage is characterized by high TVI values. It is observed also that CV metric displayed less noisier TVI image than $\bar{\mathcal{R}}_\ell$ one.

Figs. 16b) and 17b) display $\bar{\mathfrak{R}}_\ell$ and CV histograms, respectively. For TVI $= \bar{\mathfrak{R}}_\ell$, the threshold is TH $= 2.5$ while for TVI $=$ CV, TH $= 0.75$.

Fig. 16c) displays the classified leakage/non-leakage image using $\bar{\mathfrak{R}}_\ell$ metric. It can be observed that multitemporal IR analysis detected one potential leakage location. Fig. 17c) displays the classified image using CV metric. It is evident that the CV image has identified the leakage location, more accurately than that detected by the log-ratio metric.

VII. DISCUSSION

It has been demonstrated in [7] that IR camera was able to robustly detect leaks in different pipe materials and thickness(th) (PEth $= 3.5$mm, PPR th $= 5.7$mm & PVCth $= 2.6$mm) for all of the tested leak types (crack, hole & faulty joint) when the soil moisture contents were 2% and 5%. The proposed leak detection method was effective and was not affected by the thickness or the material of the pipe in all leakage types (crack, hole and faulty joint).

Since the temporal temperature variability of the leakage is higher than the shadow (see Fig. 9), the size of the shadow has not influenced the method's performance provided that the shadow was not above the leak.

Another essential characteristic of the proposed technique is the low computational complexity. For an IR image of size $Nx \times Ny$. The computational complexity of the proposed leakage detection technique is $O(Nx \times Ny \times N)$.

The proposed leak detection technique is based on the particular temporal temperature variation of the soil above the leak. In [21], it has been demonstrated that temporal temperature variation of the soil above the mines have also particular comportment. Hence, the proposed method could be easily applied to improve the detection accuracy of mines. The proposed method could be eventually applied to other similar applications.

The proposed method is an IR based technique, its limitations can be found in table 1 (see infrared thermography disadvantages). The threshold is derived after a visual analysis of the TVI histogram. After that, it is manually set to select high TVI values. As described in Table 1, this step requires a certain level of expertise to analyze the image which constitutes a limitation of the proposed method. The full automate of the proposed leak detection technique will be investigated in our future research.

VIII. CONCLUSION

In this study, soil temperature variation was determined by analyzing multitemporal IR images of leakage area in an experimental WDN setup. To mitigate the effect of time variation of field temperature, a luminance transformation was used. Results showed that the classical spatial analysis can detect water leakage areas but false positives can be observed. To address this issue, a method based on multitemporal IR analysis is proposed in this study. Using the method, the variation of soil's temperature due to field temperature was obtained and hence temperature variations due to water leakage was accurately determined.

Hence, for optimal use of IR technology, it is concluded that temporal temperature variation constitutes viable solution for water leak detection. It has been demonstrated in this study that the CV image is less noisy than the log-ratio image, and can more accurately locate the leakage. As result, the use of CV metric is recommended in further application.

REFERENCES

[1] *Ensure Availability and Sustainable Management of Water and Sanitation for All*. Accessed: Dec. 17, 2020. [Online]. Available: https://sdgs.un.org/goals/goal6
[2] K. B. Adedeji, Y. Hamam, B. T. Abe, and A. M. Abu-Mahfouz, "Towards achieving a reliable leakage detection and localization algorithm for application in water piping networks: An overview," *IEEE Access*, vol. 5, pp. 20272–20285, 2017.
[3] R. Li, H. Huang, K. Xin, and T. Tao, "A review of methods for burst/leakagedetectionandlocationinwaterdistributionsystems," *Water Sci. Technol., Water Supply*, vol. 15, no. 3, pp. 429–441, Jun. 2015.
[4] A. Awwad, M. Yahyia, L. Albasha, M. M. Mortula, and T. Ali, "Communication network for ultrasonic acoustic water leakage detectors," *IEEE Access*, vol. 8, pp. 29954–29964, 2020.
[5] A. Atef, T. Zayed, A. Hawari, M. Khader, and O. Moselhi, "Multi-tier method using infrared photography and GPR to detect and locate water leaks," *Autom. Construct.*, vol. 61, pp. 162–170, Jan. 2016.
[6] L. Ren, T. Jiang, D.-S. Li, P. Zhang, H.-N. Li, and G.-B. Song, "A method of pipeline corrosion detection based on hoop-strain monitoring technology," *Struct. Control Health Monitor.*, vol. 24, no. 6, p. e1931, Aug. 2016.
[7] H. Aslam, M. Kaur, S. Sasi, M. M. Mortula, S. Yehya, and T. Ali, "A conceptual approach to detection of water pipe leakage using non destructive techniques," in *Proc. Int. Conf. Water, Energy Environ.*, Mar. 2017, pp. 1–12.
[8] P. M. Bach and J. K. Kodikara, "Reliability of infrared thermography in detecting leaks in buried water reticulation pipes," *IEEE J. Sel. Topics Appl. Earth Observ. Remote Sens.*, vol. 10, no. 9, pp. 4210–4224, Sep. 2017,
[9] B. Shakmak and A. Al-Habaibeh, "Detection of water leakage in buried pipes using infrared technology; A comparative study of using high and low resolution infrared cameras for evaluating distant remote detection," in *Proc. AEECT*, Nov. 2015, pp. 1–7.
[10] M. Fahmy and O. Moselhi, "Automated detection and location of leaks in water mains using infrared photography," *J. Perform. Construct. Facilities*, vol. 24, no. 3, pp. 242–248, Jun. 2010.
[11] C. Penteado, Y. O. G. Lopes, P. Rodrigues, R. Filev, and P. T. Aquino, "Water leaks detection based on thermal images," in *Proc. IEEE Int. Smart Cities Conf.*, Sep. 2018, pp. 1–8.
[12] D. G. Hadjimitsis and K. T. A. Agapiou, *Detection of Water Pipes and Leakages in Rural Water Supply Networks Using Remote Sensing Techniques*, vol. 13871539. London, U.K.: InTech, 2016, doi: 10.5772/39309.
[13] C. Chatelard, "Leak detection in water transmission systems by multispectral remote sensing with airplane and UAV," in *Proc. IEEE Int. Geosci. Remote Sens. Symp.*, Jul. 2019, pp. 7124–7127.
[14] C. Chatelard, J.-C. Krapez, P. Barillot, P. Déliot, Y.M. Frérédic, J. Pierro, J.-F. Nouvel, F. Hélias, Y. Louvet, I. Legoff, and G. Serra, "Multispectral approach assessment for detection of losses in water transmission systems by airborne remote sensing," in *Proc. Int. Conf. Hydroinform.*, 2018, pp. 1–8.
[15] T. K. Chan, C. S. Chin, and X. Zhong, "Review of current technologies and proposed intelligent methodologies for water distributed network leakage detection," *IEEE Access*, vol. 6, pp. 78846–78867, 2018.
[16] J. Mashford, D. De Silva, S. Burn, and D. Marney, "Leak detection in simulated water pipe networks using SVM," *Appl. Artif. Intell.*, vol. 26, no. 5, pp. 429–444, May 2012.
[17] A. F. Colombo, P. Lee, and W. andB Karney, "A selective literature review of transient-based leak detection methods," *J. Hydro-Environ. Res.*, vol. 2, no. 4, pp. 212–227, 2009.
[18] Z. Liu and Y. Kleiner, "State of the art review of inspection technologies for condition assessment of water pipes," *Measurement*, vol. 46, no. 1, pp. 1–15, Jan. 2013.

[19] L. Boaz, S. Kaijage, and R. Sinde, "An overview of pipeline leak detection andlocation systems," in *Proc. IEEE Pan Afr. Conf. Sci., Comput. Telecommun.*, Arusha, Tanzania, Jul. 2014, pp. 133–137.
[20] R. Hidalgo-Gato, P. Mingo, J. M. López-Higuera, and F. J. Madruga, "Pre-processing techniques of thermal sequences applied to online welding monitoring," *Quant. Infr. Thermography J.*, vol. 9, no. 1, pp. 69–78, Jun. 2012.
[21] Y. Yao, M. Wen, and Y. Wang, "Multi-temporal IR thermography for mine detection," in *Proc. Int. Workshop Anal. Multitemporal Remote Sensing Images*, 2019, p. 4.
[22] D. W. Lynn, "Monotemporal, multitemporal, and multidate thermal infrared data acquisition from satellites for soil and surface-material survey," *Int. J. Remote Sens.*, vol. 7, no. 2, pp. 213–231, Feb. 1986.
[23] J. Zhao, Y. Chen, H. Feng, Z. Xu, and Q. Li, "Fast image enhancement using multi-scale saliency extraction in infrared imagery," *Optik*, vol. 125, no. 15, pp. 4039–4042, Aug. 2014.
[24] C. Ding, X. Pan, X. Gao, L. Ning, and Z. Wu, "Three adaptive sub-histograms equalization algorithm for maritime image enhancement," *IEEE Access*, vol. 8, pp. 147983–147994, 2020.
[25] H. Lu, Z. Liu, and X. Pan, "An adaptive detail equalization for infrared image enhancement based on multi-scale convolution," *IEEE Access*, vol. 8, pp. 156763–156773, 2020.
[26] Q. Fan, Y. Guo, S. Wu, and X. Liu, "Two-level diagnosis of heating pipe network leakage based on deep belief network," *IEEE Access*, vol. 7, pp. 182983–182992, 2019.
[27] M. Yahia, T. Ali, M. M. Mortula, R. Abdelfattah, and S. E. Mahdy, "Polarimetric SAR speckle reduction by hybrid iterative filtering," *IEEE Access*, vol. 8, pp. 89603–89616, 2020.

MOHAMED YAHIA received the B.Sc. degree from the Higher School of Sciences and Techniques, Tunis, Tunisia, in 2000, the M.Sc. degree from the Higher School of Communication, Tunis, in 2002, the Ph.D. degree in telecommunication engineering conjointly from the National Engineering School of Gabes (NESG), Tunisia, and the Ecole Nationale Supérieure d'Electrotechnique, d'Electronique, d'Informatique, d'Hydraulique et des Télécommunications (ENSEEIHT), Toulouse, France, in 2010, and the Habilitation degree in telecommunications from the University of Gabes, Tunisia, in 2017. Since 2018, he has been an Associate Professor with NESG. Since 2019, he has also been a Research Associate with the American University of Sharjah. His current research interests include image processing, analysis of synthetic aperture radar images, and numerical methods in electromagnetism.

RAHUL GAWAI received the M.Sc. degree in geoinformatics and the P.G.B.Sc. degree in geographical information system (GIS) and remote sensing from the University of Pune, India. He worked in multidisciplinary subjects, such as health science, geology, zoology, botany, and watershed management in the field of GIS and remote sensing. He has more than ten years' experience in GIS and remote sensing. Prior to joining AUS, he worked for various GIS and government organizations in India and United Arab Emirates. He also has experience teaching in GIS and remote sensing at the Department of Geography, Savitribai Phule Pune University, formerly the University of Pune. His research interests include GIS, data science, python, ESRI dashboard, drone mapping, remote sensing, ArcGIS online, 3-D GIS and adobe creative cloud, and among other areas.

TARIG ALI (Senior Member, IEEE) received the B.S. degree (Hons.) in civil engineering from the University of Khartoum, Sudan, in 1993, and the M.S. and Ph.D. degrees from The Ohio State University, USA, in 1999 and 2003, respectively. He is currently a Professor with the American University of Sharjah. His research interests include geospatial engineering, GIScience, coastal mapping and GIS, and applications of GIS and remote sensing in civil and environmental engineering.

MD. MARUF MORTULA received the B.Sc. degree from the Bangladesh University of Engineering and Technology, Bangladesh, in 2000, and the M.Sc. and Ph.D. degrees from Dalhousie University, Canada, in 2002 and 2006, respectively. Since 2018, he has been a Full Professor with the American University of Sharjah. His research interests include water and wastewater treatment, recycling of solid waste management, water quality management in coastal water, and water infrastructure management.

LUTFI ALBASHA (Senior Member, IEEE) received the B.Eng. and Ph.D. degrees in electronic and electrical engineering from the University of Leeds, U.K. He joined Sony Corporation, in 1997, where he was involved in commercial RFIC chip products for mobile handsets. He joined Filtronic Semiconductors, in 2000, as a Senior Principal Engineer, where he created an IC Design Team. The team supported the company foundry design enablement for mass production of RFIC products and taped-out its first commercial chips. This becomes a very successful business in Europe's largest GaAs MMIC foundry. He returned to Sony as a Lead Principal Engineer, where he was involved in highly integrated RFCMOS and BiCMOS transceivers for cellular and TV applications. He joined the American University of Sharjah, where he is currently an Associate Professor of Microelectronics. His current research interests include energy harvesting and wireless power transfer, low-power wearable and implantable devices, power amplifier design and linearization for multi-band multimode applications, and integrated radar transceivers. He received several outstanding recognition awards from Sony Corporation, IET, and the University of Leeds. He is also an Associate Editor of the *IET Microwaves, Antenna & Propagation* journal and also serves as the President for the UAE Chapter of the IEEE Solid-State Circuits Society.

TAHA LANDOLSI received the Ph.D. degree from The University of Texas at Dallas, USA, in 1999. He worked in the telecommunications industry for more than seven years, designing and planning wireless and optical networks in several U.S. markets. He is currently a Professor of Computer Engineering with the American University of Sharjah, United Arab Emirates. His research interests include wireless and optical networks and optical devices and materials.